# Influence of filler on the microstructure, mechanical properties and residual stresses in TIG weldments of dissimilar titanium alloys

Massab Junaid[1], Fahd Nawaz Khan[2]*, Tauheed Shahbaz[2], Haris saleem[2], Julfikar Haider[3]

[1] Faculty of Mechanical Engineering, Ghulam Ishaq Khan Institute of Engineering Sciences and Technology, Topi 23640, Pakistan

[2] Faculty of Materials and Chemical Engineering, Department of Materials Science, Ghulam Ishaq Khan Institute of Engineering Sciences and Technology, Topi 23640, Pakistan

[3] Advanced Materials and Surface Engineering (AMSE) Research Centre, Manchester Metropolitan University, Chester Street, M1 5GD, UK

* Corresponding author: Professor Fahd Nawaz Khan; Telephone: 0092 336 9151127; Email: fahd@giki.edu.pk

**Abstract**

The influence of titanium alloy (Ti-5Al-2.5Sn) and commercially pure titanium (cpTi) as fillers on dissimilar pulsed TIG weldments of Ti-5Al-2.5Sn/cpTi was investigated in terms of microstructure, mechanical/nano-mechanical properties, and residual stresses. A partial martensitic transformation was observed in the weldments for all the welding conditions due to high heat input. The microstructure evolved in the FZ/cpTi interfacial region was observed to be the most sensitive to the proportion of α stabilizer in the filler alloy. Furthermore, the addition of filler alloy improved the tensile properties and nano-mechanical response of the weld joint owing to the increased volume of metal in the weld joint. As compared to the Ti-5Al-2.5Sn wire, the use

of cpTi filler wire proved to be better in terms energy absorbed during tensile and impact tests, tensile strength and ductility of the dissimilar welds. An asymmetrical residual stresses profile was observed close to the weld centerline, with high compressive stresses on the Ti-5Al-2.5Sn side for both the weldments obtained with and without filler wires. This was attributed to mainly the low thermal conductivity of Ti-5Al-2.5Sn. The presence of residual stresses also influenced the nano-hardness profile across the weldments in terms of magnitude.

**Keywords:** Titanium alloys; Dissimilar welding; Nanoindentation; Residual stresses; TIG welding; Microstructure

## 1. Introduction

Titanium alloys are well known to possess excellent strength to density ratio, high corrosion resistance and good bio-compatibility. These attractive properties have led to titanium alloys being used in industries where the weights of the components are crucial or in the areas of corrosive environments. Szusta et al. [1] have reported that marine, aerospace, petrochemical related industries, frequently use titanium and its alloys in critical applications. Furthermore, owing to their high biocompatibility, titanium alloys are used for medical implants as reported by Koizumi et al. [2]. However, according to Froend et al. [3], one of the key concerns in welding of titanium alloys is its susceptibility to environmental contamination, which makes it difficult to weld as compared to the welding of conventional structural alloys such as steels and aluminum alloys. Almost all types of welding operations have been carried out on titanium alloys. e.g., tungsten inert gas (TIG), laser beam welding (LBW), electron beam welding (EBW) and friction stir welding [1,4–16]. In order to overcome the contamination issue in welding of titanium alloys, an inert gas is traditionally used during welding [17–19].

2

The purpose of welding dissimilar titanium alloys is to achieve the desired properties of both the alloys in a single component in an economical way. For example, Froend et al. [3] reported that in aerospace industry, commercially pure titanium (cpTi) is mostly used as an outer skin material, whilst Ti-6Al-4V is generally chosen as stiffening stringer material. The challenges in welding dissimilar titanium alloys include the problems encountered in welding of the base alloys individually, as well as understanding the incompatibility issues arising due to the range of compositional gradients. This leads to large variations in physical and mechanical characteristics across the weldments.

A number of studies have been conducted to investigate the weldments of dissimilar titanium alloys such as cpTi/Ti-6Al-4V[20], Ti-6Al-4V/Ti17[21], TC17/TC60[22], Ti-22Al-25Nb/TA15[23], Ti–22Al–27Nb/TA15[24], Ti-6Al-4V/Ti-4.5A1-3V-2Fe-2Mo[25], Ti–22Al–25Nb/TC11[26], Ti-6Al-4V/Ti17,Ti-6Al-4V/BT9[27] and $Ti_3Al$/Ti-6Al-4V[28]   using various techniques e.g., LBW, EBW and TIG-Laser hybrid welding. For instance, Wang et al. [27] studied electron beam weldments of Ti-6Al-4V/Ti17 and Ti-6Al-4V/BT9  dissimilar alloys and reported an increased joint strength relative to the base alloys. Zhang et al. [28] performed EB welding of two dissimilar titanium alloys, $Ti_3Al$ and TC4 and found the tensile strength to be approximately 92% of the $Ti_3Al$ base alloy. Similarly in the work by Tan et al. [26] related to EBW of Ti–22Al–25Nb/TC11 dissimilar alloys, the tensile strength of the joint was reported to be higher than the TC11 base alloy. However, they observed that the heat affected zone (HAZ) exhibited lower micro-hardness as compared to the Ti–22Al–25Nb base alloy, owing to the presence of softer B2 phase. This also led to a reduction in impact toughness of the joint, which was approximately 42% of the TC11 base alloy.

In addition to the observation of Tan et al., a number of other researchers reported weld zone softening in dissimilar titanium alloys weldments resulting in degradation of mechanical properties. For instance, Li et al [23] carried out dual laser welding of dissimilar titanium alloys, namely Ti-22Al-25Nb and TA15. They observed B2 and O phases in the fusion zone resulting in a significant reduction of its microhardness. Furthermore, they also observed that the fractured surfaces of tensile specimens possessed even and deep dimples suggesting a softer fusion zone. Similarly Zhang et al. observed that the fusion zone of Ti–22Al–27Nb/TA15 dissimilar TIG-laser hybrid weldment had a reduced microhardness due to the formation of soft B2 phase [24]. To address this issue, Chu et al. proposed post weld heat treatment (PWHT) of the dissimilar weld joints. They investigated the influence of PWHT on the properties of $CO_2$ laser weldments of Ti-6Al-4V/Ti-4.5A1-3V-2Fe-2Mo dissimilar alloys and concluded that the FZ properties could be significantly improved using PWHT [25]. Beam offsetting technique was also employed in beam welding processes such as EBW and LBW of dissimilar titanium alloys. In this method, the contribution of each base metal can be adjusted by offsetting the beam to vary the properties in the dissimilar weld zone. This was observed by Zhang et al. [29] who performed LBW on BTi-6431S/TA15 dissimilar titanium alloys and by Liu et al [30] who carried out LBW of Ti-6-4/Beta-C titanium alloys. Similarly, Yeganeh and Li [31] reported the effect of beam offsetting on the microstructure and mechanical properties of Ti55/TA15 dissimilar weldments processed by EBW.

Another possible solution to address the issue of weld zone softening in dissimilar titanium alloy weldments could be altering the chemistry of the weld zone by addition of a filler and this approach has been successfully applied in welding titanium alloys to other alloys such as steels [32,33]. For instance, Chu et al. [32] performed TIG welding of TA1 and Q235 steel using V, ER 50-6 and ERTi-1 as fillers and observed good bonding characteristics of V with Ti and Fe.

Similarly, Tomashchuck et al. [33] addressed the issue of brittleness in electron beam and laser beam weldments of Ti6Al4V/AISI 316L using a copper interlayer. It would be therefore of prime interest to investigate the influence of different fillers (cpTi and Ti-5Al-2.5Sn) on the dissimilar cpTi/Ti-5Al-2.5Sn TIG weldments which is the objective of the present study. The cpTi/Ti-5Al-2.5Sn dissimilar welding can be targeted for applications in the integrated engines where the requirement is to join relatively high temperature titanium alloy with low-temperature, low-cost titanium alloys [27]. Such an approach can also produce structures for aerospace industry requiring high temperature strength along with good formability. Moreover, recently there is a great deal of interest in the selection of appropriate fillers which can induce compressive strains in the fusion zone due to solid state transformations [34]. The present work will also investigate on selecting the suitable candidate between the fillers (cpTi and Ti-5Al-2.5Sn) from the aspects of microstructure, mechanical/nano-mechanical properties and residual stresses of the weldments.

## 2. Materials and experimental conditions

### 2.1 Sample preparation

Two α titanium alloys (cpTi and Ti-5Al-2.5Sn) were used in the present study as base materials (BM). The chemical composition of Ti-5Al-2.5Sn alloy is 5.34 Al, 2.56 Sn, 0.27 Fe, 0.17 O, 0.02 V, 0.03 Si, 0.01 C, 0.01 N and balance Ti, whereas the chemical composition of cpTi is 0.02 N, 0.08 C, 0.007 H, 0.18 Fe, 0.15 O, and Ti balance. Both alloys were also used as individual filler during welding operation. Sheet of CP Ti and Ti-5Al-2.5Sn, with a thickness of 1.6 mm were sectioned into rectangular coupons with a nominal dimension of 75 mm × 50 mm. Prior to welding, the coupons were cleaned using ethanol, in order to remove any contamination. Automatic pulsed TIG welding was performed to join the coupons of the dissimilar titanium alloys, in a butt configuration to obtain a weldment with a final dimension of 75 mm × 100 mm. Welding was

performed under a constant flowrate of argon gas (12 L/min), with fillers and without a filler. The filler metal was in the form of a wire with a diameter of 1 mm and was fed at a speed of 40 mm/min. The welding parameters and other operating conditions are given in Table 1 and against each of the welding conditions, three weldments were obtained for further characterization.

## 2.2 Microscopic observation

Wire EDM was used to prepare metallographic and tensile testing specimens from the weldment. Samples were ground using SiC papers from 200 to 5000 grit size in steps and the final polishing was performed using 2.5 and 1 µm diamond paste. In order to etch both cpTi and Ti-5Al-2.5Sn alloy and the weldment, Kroll's reagent (92 ml of $H_2O$, 2 ml of HF and 6 ml of $HNO_3$) was used. Microscopic observations were performed by using OLYMPUS BH2-UMA polarized optical microscope with a sensitive tint filter. MIRA3 Tescan Scanning Electron Microscope (SEM), equipped with Energy Dispersive X-ray Spectroscopy (EDS) was used for microstructural imaging and chemical analysis.

## 2.3 Mechanical/nano-mechanical tests

A 30 kN Instron machine was used for tensile testing at room temperature. ASTM standard E8M-04 was followed for smooth tensile testing and ASTM standard E338-03 was followed for double notch tensile testing (a notch angle of $60^o$ with a notch depth of 2.5 mm). Micro hardness measurements across the weld zone were carried out on the metallographic samples using Tukon Model 300 Vickers hardness machine. An indentation load of 200 gf was applied for a holding time of 10 s and the distance between two indents was maintained at 0.5 mm.

iMicro Nano indenter (made by *Nanomechnaics, Inc USA*) was used to measure the nano mechanical characteristics such as load-displacement curves, elastic modulus and nano hardness. Berkovich tip was used for indentation purposes and in total 20 indentations were made on each

sample starting from cpTi to Ti-5Al-2.5Sn alloy side while passing through the weld zone. All indentations were carried out at a maximum load of 500 mN, under the continuous stiffness mode.

## 2.4 Residual stress measurement

The residual stresses were measured in the weldments, on both the sides of the weld line using hole drill strain measurement setup (HDSM). A hole of 1.6 mm was drilled at the center of each strain gauge rosette installed at a location of 5 mm away from the weld line. A high-speed pneumatic drilling operation was performed at a very slow feed rate, in an intermittent pattern. As a result of this drilling operation, strains were relieved which was recorded by the Vishay P3 data acquisition system interfaced with the strain gauge rosette. A number of standards such as ASTM E837 and those by Micro measurements systems such as B-127-4, TT-603, TT-606, TT-609 were followed in the residual stress measurement using HDSM. The residual stresses in the welding and transverse direction were computed by processing the acquired strain data using the integral method approach in the Hdrill software.

## 3. Results and Discussions

### 3.1 Physical appearance

The top surfaces of the weldments corresponding to all three welding conditions are shown in Fig. 1. It can be seen that the weld beads are of shinny appearance, indicative of no contamination. This is of significant importance especially for titanium alloys because of their high reactivity towards atmospheric oxygen at elevated temperature. Furthermore, this suggested that the flow of shielding gas was sufficient enough to prevent any oxidation.

### 3.2 Microstructural evolution

Microstructures of the two base alloys, in the as-received condition are shown in Fig. 2. It can be seen that both the alloys were predominantly of equiaxed α grains in a prior β matrix,

however, the grains were much coarser in cpTi. The average grain size as measured through ImageJ software in cpTi base alloy was approximately 9.3 µm, whereas in Ti-5Al-2.5Sn alloy, it was significantly less (approximately 1.6 µm). Similar microstructure have been reported for Ti-5Al-2.5Sn alloy by Tan et al.[35] and by Amaya-Vazquez et al.[10] for cpTi.

The microstructural analysis across the weld zone revealed some very interesting results. Fig. 3 shows that for all the three welding conditions, the fusion zone (FZ) microstructure was predominantly comprised of acicular α and α' martensite, which is suggestive of a cooling rate higher than 410 $^\circ$C$^{-1,}$ required to achieve diffusionless transformation from β to α [36]. The presence of prior β grains in the FZ of the three weldments is owing to the low thermal conductivity of titanium alloys and the high heat input of the TIG welding processes, indicating a partial martensitic transformation. These prior β grain boundaries were not observed in the LBW of Ti-5Al-2.5Sn (as reported by Junaid et al., 2017 [11]) alloy due to the fact that the power density of laser heat source in LBW was in the same range as the electron beams in EBW. However, the flow of shielding gas in LBW enhanced the cooling rate and therefore a complete martensitic transformation occurred [4,11,18].

Adjacent to the FZ are the two HAZs: one towards each side of the BM (Ti-5Al-2.5Sn and cpTi), in which the evolution of microstructure (prior β grain size, acicular α and α' martensite) is dependent on a number of factors. An analysis of these factors helps in further understanding of the physical phenomenon taking place during the welding process. The HAZ region for the three welding conditions are shown in Fig. 4 and Fig. 5. The increase of prior β grain size while moving from BM (cpTi: 4.5µm and Ti-5Al-2.5Sn: 1.7 µm) to the HAZ (cpTi side no filler:13 µm, cpTi side Ti-5Al-2.5Sn filler: 12.8 µm, cpTi side cpTi filler: 7.8 µm, Ti-5Al-2.5Sn side no filler:9.2 µm, Ti-5Al-2.5Sn side Ti-5Al-2.5Sn filler: 8.6 µm, Ti-5Al-2.5Sn side cpTi filler: 8.7 µm,  )and

FZ (no filler: 18 µm, Ti-5Al-2.5Sn filler: 16.5 µm, cpTi filler: 16.7 µm) can be observed for all the three welding conditions. Since both the titanium alloys under consideration have a low thermal conductivity, the heat absorbed during the welding process favored grain growth in the HAZ. Such observation have also been reported in the independent work performed on the welding cpTi by Karpagharaj et al. [18] and for TI-5Al-2.5Sn alloy by Junaid et al. [12].

A comparison of Fig. 5 and Fig. 6 shows that the extent of martensitic transformation (fine needle like microstructure) was more significant in the HAZ towards Ti-5Al-2.5Sn side of the weldments (HAZ:Ti-5-2.5 as compared to the HAZ towards cpTi side (HAZ:cpTi) for both filler conditions. During the heating stage of welding cycle, the HAZ towards both the parent alloys experienced temperature less than the melting points of the base alloys, but still higher that the β transus temperature due to which, α was completely transformed to β. However, during the subsequent cooling cycle, the reverse transformation of β to α depends on the cooling rate [37] and the amount of α or β stabilizers[38]. It has been reported that an increase in cooling rate and the presence of α stabilizers favors the formation of acicular α and martensitic α' [29]. The presence of Al in Ti-5Al-2.5Sn alloy serves this purpose and increases the martensitic initiation temperature ($M_s$) [39]. Hence, during cooling cycle, β to α transformation starts at a relatively higher temperature, favoring the stabilization of α' at room temperature. This was also evident from the increased size of the prior β grains in HAZ:cpTi owing to heat retention as compared to the grains in HAZ:Ti-5-2.5. Furthermore, the inclusion of filler alloys significantly affects the formation of martensite in the HAZ towards cpTi side of the weld joint. This can be observed by comparing Fig. 5a with Fig. 5b and Fig. 5c in which martensitic features can only be observed in HAZ towards cpTi side of the weldment obtained without filler which can be attributed to the expected higher cooling rates in this case [36]. Owing to the enhanced volume of molten material

in the weldment, which is due to the presence of filler, the peak temperatures attained were less than the weldment obtained without any filler. Consequently, the cooling rates in the weldments developed with filler was less than that of the weldment obtained without filler.

### 3.3 Micro hardness profile

The variation of microhardness in different welding regions for all the welding conditions is presented in Fig. 6. There is a significant difference between the microhardness of the two BM, owing to the alloying additions in Ti-5Al-2.5Sn alloy (320 HV for Ti-5Al-2.5Sn as compared to 160 HV for CPTi). It is clear that the microhardness increases with the inclusion of Ti-5Al-2.5Sn filler and for the weldments obtained without any filler material.

A number of factors could be responsible for the observed variations in the microhardness profiles across the weldments. The prime factor contributing towards the increase in the microhardness while moving from the BM to the FZ is the formation of martensitic microstructure, which is harder than the equiaxed α phase present in both the BMs [37]. The formation of this needle like α' martensite in the fusion zone is a diffusionless transformation, which is dependent on the cooling rate. The FZ experienced peak temperature far above the melting point during the welding process, thereby leading to high temperature gradients upon cooling. The observed higher cooling rates in the FZ lead to greater proportion of α' martensite and therefore resulting higher hardness as concluded by Wu et al. [13].

The second factor is the addition of filler in the weldment. In the present study, the two filler alloys have a significant difference in Vickers hardness. For Ti-5Al-2.5Sn, the micro-hardness was measured to be approx. 320 HV whereas for cpTi, it was approx. 150 HV. While moving from the Ti-5Al-2.5Sn side of the BM towards the FZ, the influence of cpTi resulted in lowering the micro hardness as compared to the expected value. This behavior can also be observed

10

by comparing the FZ hardness with the study on Ti-5Al-2.5Sn similar welds[14] in which micro hardness of the FZ was found to be approximately 370 HV as compared to the 340 HV in the present work. A similar trend is observed for the weldment obtained with Ti-5Al-2.5Sn as filler.

There is also a significant influence of the alloying composition on the micro-hardness profile of a dissimilar titanium alloy weldment. For a given titanium alloy, the response to thermo-mechanical processing depends on the Mo and Al equivalents ($Mo_{EQ}$ and $Al_{EQ}$) values. The conversion of different alloying elements into Mo and Al equivalents is given by the following equations [15].

$$[Al]_{EQ} = [Al] + \frac{[Zr]}{6} + \frac{[Sn]}{3} + 10[O] \tag{1}$$

$$[Mo]_{EQ} = [Mo] + \frac{[Ta]}{5} + \frac{[Nb]}{3.6} + \frac{[W]}{2.5} + \frac{[V]}{1.5} + 1.25[Cr] + 1.25[Ni] + 1.7[Co] + 1.7[Mn] +$$

$$2.5[Fe] \tag{2}$$

Hsieh et al. [16] reported that the weldments of dissimilar alloy combination with a higher value of $Mo_{EQ}$ showed a higher micro hardness in the as welded (AW) condition [16]. For instance, for Ti-6-4/Ti–6.5Al–3.5Mo–1.5Zr–0.3Si, the $Mo_{EQ}$ values of the two alloys were in the range of 3.5 and the resultant Vickers hardness was observed to be upto 370 HV [5]. Similarly, for Ti-6-4/Ti–5Al–4Mo–2Zr–Cr–2Sn–0.3Fe dissimilar joint (Max $Mo_{EQ}$ of 9.7), the maximum microhardness was observed to be 425 HV. In the present study, since no $Mo_{EQS}$ were present in both the cpTi and Ti-5Al-2.5Sn alloy under study, the observed microhardness in the FZ was not significantly higher than the BM (Ti-5Al-2.5Sn).

During the post weld cooling cycle, the extent of β to α transformation in the FZ and HAZ of the weldments can be quantified, to some extent from the microhardness profile of the

weldments as shown in Fig. 6. Since an increased hardness in the FZ and HAZ is owing to the formation of α' martensite and acicular α, the difference between the FZ microhardness for different conditions of filler can be correlated to the amount of these phases present in the weldment [36,37]. The highest FZ microhardness corresponding to the weldments obtained without any filler suggested the highest cooling rate and therefore higher proportion of martensitic transformation in the FZ. This also corroborates the hypothesis of increased cooling rate, due to less amount of molten metal in the weld pool, for the same conditions of heat input resulting in higher peak temperatures as compared to the weldments obtained with filler.

**3.4 Tensile strength**

Fig. 7 shows the influence of adding filler on the smooth tensile behavior of the dissimilar weldments. Table 2 can be referred for the exact values of the load, total energy and extension at break. All the samples fracture through the BM of CPTi side of the BM. This was owing to low yield strength of CPTi (371.8 ± 5.7) as compared to the Ti-5Al-2.5Sn (823 ± 4.1). It is clear that the weldments obtained using cpTi as filler exhibited highest elongation and energy absorbed before fracture, followed by the weldments obtained using Ti-5Al-2.5Sn as filler. This was owing to the inherent formability characteristics of cpTi, which is less in the case of Ti-5Al-2.5Sn due to the alloying addition. Furthermore, it can be observed that the addition of filler in the weldment improved tensile properties of the dissimilar cpTi/Ti-5Al-2.5Sn joint as compared to the joint obtained without using filler wire. This can be attributed to an enhanced penetration in the weld joint, owing to the increased volume of the molten pool resulting from the filler material at the cpTi/Ti-5Al-2.5Sn interface. The enhanced elongation of the weld joint obtained with filler can also be attributed to a reduction in micro-crack formation in weld zone owing to the presence of the filler alloys (Ti-5Al-2.5Sn and cpTi) in the molten pool. Several studies are available in the

12

literature concerning the beneficial effects of filler addition in terms of micro-cracks suppression. The work by Kelly et al. on Inconel 718 alloy and filler, Saida et al. and Saida et al. on the use of Ce and La based fillers in welding of steels suggested different mechanisms responsible for the suppression of micro-cracks in the weldments [40–42]. Depending on the type of filler and the base alloy, these mechanisms could be: the formation of coarse interdendritic phase network [40], segregation of impurities [41] or the enlargement of brittle temperature range (BRT) [42]. The precise phenomenon of the influence of filler addition on the micro-crack suppression in the titanium alloy weldments requires further investigation.

In order to further investigate the evolution of FZ microstructures, the double notch tensile specimens (NTS) with notch located at the FZ were prepared. The tensile behavior (Fig. 8 and Table 3) and corresponding fracture morphology (Fig. 9) provides further understanding of the strengthening mechanism in the FZ. It can be observed that the size of the dimples in the Fig. 9(c) is significantly smaller than the size of dimples in Fig. 9(a) and Fig. 9(b). These relatively small sized dimples are responsible for the increase in overall energy absorbed by the NTS samples of the weldments with cpTi filler by approximately 80% to that of the weldments obtained with Ti-5Al-2.5Sn filler [6]. Moreover, the increased ductility of weldments with cpTi filler could be due to less amount of martensite in the weld zone. According to Balasubrimanian et al. [19], the formation of martensite in the weld zone in titanium alloys increased its strength and micro-hardness, but reduced its elongation. Hard and brittle fusion zone may have a high value of elastic modulus (Table 3) but the premature failure reduced the overall absorbed energy [6].

**3.5 Nano-mechanical response of the weldments**

To further understand the influence of filler and the variation of mechanical behavior across the weldments, the load-depth (P-h) curves of the nano-indentation were plotted. These curves can

be used to predict both the stress-strain relationship as well as the hardness properties at the grain level. Fig. 10 compares the nano-mechanical response of the two base alloys, which shows a more significant depth of penetration for cpTi as compared to Ti-5Al-2.5Sn alloy. The resultant nano-hardness was measured to be 2 GPa for cpTi and 4.5 GPa for Ti-5Al-2.5Sn alloy. Similarly, the elastic moduli were measured to be 103±2 GPa and 136±4 GPa for cpTi and Ti-5Al-2.5Sn alloy respectively.

Fig. 11, Fig. 12 and Fig. 13 show the P-h curves of the indents in HAZ and FZ of the Ti-5Al-2.5Sn/cp-Ti dissimilar weldments obtained without filler, with cpTi filler and with Ti-5Al-2.5Sn filler respectively and the results are summarized in Table 5. Nano-hardness and elastic modulus were calculated using post processing of the data of these load-depth curves, using the Oliver and Pharr method [43]. It can be observed that there is a significant variation in P-h curves in the HAZ and BM region of the weldments, which can be attributed to the extent to which different phases were present in the microstructure and the state of residual stress near the weld centerline.

A comparison of Fig. 6 and Table 4 shows a contrasting trend in the Vickers hardness and nano-harndness of the FZ and HAZ of dissimilar weldments obtained under different conditions of filler alloys. This trend is owing to the fact that there is a strong relationship between residual stresses and nano-hardness whereas the microhardness is not significantly affected by the state of residual stresses. The experiments performed by Kokubo in 1932, showed that a state of compressive stress do not significantly affects the Vickers hardness in most of the alloys [44]. Nano-hardness, on the other hand is significantly affected by the presence of residual stresses and is increased in a compressive state of stress[45]. For the weldments obtained without any filler, an increasing trend in the micro hardness was observed while moving from BM to FZ (12% increase

14

in the FZ as compared to BM) in contrast to its nano-hardness which exhibited a decreasing trend (40% decrease in the FZ as compared to BM). This was owing to the state of tensile residual stress near the weld line. The weldments obtained with Ti-5Al-2.5Sn as filler had a lower FZ microhardness as compared to the FZ of the weldments with no filler, which was attributed to the increased proportion of hard phases in the later as discussed in section. On the contrary, nano-hardness in FZ of weldments obtained with Ti-5Al-2.5Sn as filler was higher than that of the weldments with no filler. This was owing to the increased amount of the material capable of producing compressive strains (both Ti-5Al-2.5Sn filler and Ti-5Al-2.5Sn BM) in the former. This state of compressive stress increased the apparent force required for nanoindentation, thus increasing its nano-hardness.

### 3.6 Residual stress distribution

Residual stresses are generated in the weldments due to a number of factors: plastic flow of metal, the differential cooling rate within the FZ and HAZ owing to the different level of heat input and the phase transformations during the solidification of weld pool [46]. During the joining process, the weld centerline experiences extremely high temperatures in the heating cycle due to which the weldzone expands significantly along the centerline (longitudinal direction) and partly in the transverse direction. During the cooling cycle, the weld metal contracts, however since it is connected with the parent metal, the weldzone shrinkage induces tensile strains. Moreover, it has been observed by Rossini et al[46] that compressive strains are induced in the adjacent base material during this cooling cycle. Any phase transformation within the weldzone during this process will induce additional strains, the nature of which is dependent on the type of phases formed [34]. These welding related induced residual stresses can induce brittle fracture, stress corrosion and buckling deformation thereby reducing the welded components life [47]. In the

15

present work, both longitudinal and transverse residual stresses were measured on both sides of the weld centerline and results are presented in Table 5. For all the conditions of filler alloys, the residual stresses are less towards the cpTi side of the weld centerline, owing to the low yield strength of cpTi (340 MPa) as compared to the Ti-5Al-2.5Sn alloy (827 MPa) (www.matweb.com). Furthermore, owing to the slight difference between the coefficient of thermal expansions (9.4 µm/m-°C for Ti-5Al-2.5Sn as compared to 8.6 µm/m-°C for cpTi), (www.matweb.com), the corresponding shrinkage in the cooling cycle would be more towards Ti-5Al-2.5Sn side of the weldment. This phenomenon should have induced compressive residual strains on the cpTi side of the weldment. However, the observed residual stresses were found to be compressive towards the Ti-5Al-2.5Sn side. This anomaly can be attributed to the higher thermal conductivity of cpTi (16.4 W/m.K) as compared to the Ti-5Al-2.5Sn (7.8 W/m.K). Owing to the significant difference in the thermal conductivities of the two alloys (almost double), heat flow was more towards cpTi (with higher thermal conductivity 16.4 W/m.K) side of the weldment resulting in a significant expansion and the subsequent shrinkage of the cpTi side of the plate during the cooling stage. This shrinkage in cpTi alloy induced compressive strains on the Ti-5Al-2.5Sn side resulting in a high value of compressive stresses which was not observed in autogenous welds of Ti-5Al2.5Sn alloy [12,14].

It can be further observed in Table 5, that the weldments obtained without filler exhibited the highest tensile residual stresses. As discussed earlier, the energy required to melt the filler alloy reduced the overall heat input which significantly decreases the tensile residual stresses. In welding of thin sheets, the tensile residual stresses are mainly produced due to weld line contraction and is observed to be directly related to the overall heat input of the process [46]. For instance, in general, TIG welding process induces a higher degree of tensile residual stresses as compared to the LBW,

owing to the overall higher heat input required in the former to achieve a full penetration[48]. In titanium alloys, compressive residual stresses can also be generated due to an increase in the local volume of the weldzone, owing to the β to α transformations during the cooling cycle of the joining process[49]. It has also been stated that α stabilizers further promote this phase transformation [29]. Moreover, the inclusion of fillers also affects the martensitic initiation temperature ($M_s$) which influences the overall proportion of martensite in the weld zone[50]. For instance, an increase in $M_s$, leads to the start of β to α' transformations at relatively higher temperatures thereby leading to higher proportions of martensite in the weld zone and consequently generating a higher level of compressive stresses. However, increase in $M_s$ beyond a certain limit can also result in the phase transformation to complete early and tensile stresses will be generated during further shrinkage of the weldment until the ambient temperature is reached[50]. For this reason, the compressive residual stresses are the highest in the weldments obtained with Ti-5Al-2.5Sn filler material which can be attributed to the presence of Al (an α stabilizer)[39], thus promoting the formation of α' martensite. Moreover, as discussed earlier, the decrease in heat input due to the addition of filler alloy opposed the generation of tensile residual stresses which further intensified the state of compressive residual stress in the weldments obtained using Ti-5Al-2.5Sn filler.

## 4. Conclusions

In the present work, TIG welding operation was employed to join Ti-5Al-2.5Sn and cpTi alloys, both of which have a significant difference in microstructure, microhardness and physical properties. Selection of the appropriate filler alloys was also part of the present study, since they influence the phase transformation in the weld zone. The following conclusions were drawn after detailed investigation:

1. Owing to the high heat input involved in TIG welding process, a partial martensitic transformation in the FZ and a significant increase in prior beta grain size in the FZ and HAZ was observed for all the three welding conditions (no filler, Ti-5Al-2.5Sn and cpTi as fillers).

2. Several factors related to welding of dissimilar titanium alloy weldments, using filler alloy, influenced the evolution of weld zone (HAZ and FZ) microstructure, the most dominating being the proportion of alpha stabilizer in the filler and base alloys. Owing to this, acicular α and α' martensite in relatively fine beta grain matrix were observed in the HAZ towards Ti-5Al-2.5Sn side of the BM, which was absent in the HAZ towards cpTi side.

3. The highest microhardness was observed in the weldments obtained without filler, despite the absence of the alpha stabilizers. This was attributed to the reduced volume of the molten metal in the weld pool. On the contrary, the welds with cpTi filler possessed the highest elongation and energy absorbed during tensile tests.

4. The residual stresses exhibited an asymmetric pattern across the weldment, with higher stresses towards Ti-5Al-2.5Sn side, which were mainly compressive in nature. The highest level of compressive stress was observed in the weldment obtained with Ti-5Al-2.5Sn alloy as filler, having the highest proportion of α stabilizers, which may have increased the martensitic initiation temperature in the weld zone. Thermal conductivity of the base materials also played a major role in the residual stress distribution across the weldments and induced compressive stresses towards the alloy having lower thermal conductivity (Ti-5Al-2.5Sn).

5. Owing to a state of tensile residual stress in the weldments obtained without filler, an increasing trend in microhardness, while moving from BM to FZ was observed as compared to a decreasing trend in nano-hardness, whereas a state of compressive stresses induced an opposite behavior in the weldments obtained with the Ti-5Al-2.5Sn filler.

**References**

1. J. Szusta, N. Tüzün, and Ö. Karakaş, Theor. Appl. Fract. Mech. 100, 27 (2019).

2. H. Koizumi, Y. Takeuchi, H. Imai, and T. Kawai, J. Prosthodont. Res. (2019).

3. M. Froend, F. Fomin, S. Riekehr, P. Alvarez, F. Zubiri, S. Bauer, B. Klusemann, and N. Kashaev, Opt. Laser Technol. 96, 123 (2017).

4. A. B. Short, Mater. Sci. Technol. 25, 309 (2009).

5. S. Q. Wang, J. H. Liu, and D. L. Chen, Mater. Sci. Eng. A 584, 47 (2013).

6. W. Zhou and K. G. Chew, Mater. Sci. Eng. A 347, 180 (2003).

7. G. Q. Wang, Z. B. Zhao, B. B. Yu, J. R. Liu, Q. J. Wang, J. H. Zhang, R. Yang, and J. W. Li, Acta Metall. Sin. (English Lett. 30, 499 (2017).

8. H. J. Yi, Y. J. Lee, and K. O. Lee, Acta Metall. Sin. (English Lett. 28, 684 (2015).

9. M. Junaid, F. N. Khan, N. Baksh, M. N. Baig, and K. Rahman, Mater. Des. 139, 198 (2018).

10. M. R. Amaya-Vazquez, J. M. Sánchez-Amaya, Z. Boukha, and F. J. Botana, Corros. Sci. 56, 36 (2012).

11. M. Junaid, F. N. Khan, K. Rahman, and M. N. Baig, Opt. Laser Technol. 97, 405 (2017).

12. M. Junaid and F. N. Khan, Proc. Inst. Mech. Eng. Part L J. Mater. Des. Appl. 0, 1 (2018).

13. M. Wu, R. Xin, Y. Wang, Y. Zhou, K. Wang, and Q. Liu, Mater. Sci. Eng. A 677, 50 (2016).

14. M. Junaid, M. N. Baig, M. Shamir, F. N. Khan, K. Rehman, and J. Haider, J. Mater. Process. Technol. 242, 24 (2017).

15. C. T. Hsieh, R. K. Shiue, R. Huang, and L. W. Tsay, 653, 139 (2016).

16. C. T. Hsieh, C. Y. Chu, R. K. Shiue, and L. W. Tsay, J. Mater. 59, 227 (2014).

17. X. L. Gao, L. J. Zhang, J. Liu, and J. X. Zhang, Mater. Sci. Eng. A 559, 14 (2013).

18. A. Karpagaraj, N. Siva, and K. Sankaranarayanasamy, Mater. Sci. Eng. A 640, 180 (2015).

19. V. Balasubramanian, V. Jayabalan, and M. Balasubramanian, Mater. Des. 29, 1459 (2008).

20. F. Fedor, M. Froend, V. Ventzke1, P. Alvarez, S. Bauer, and K. Nikolai, Int. J. Adv. Manuf. Technol. 97, 2019 (2019).

21. S. Q. Wang, J. H. Liu, and D. L. Chen, Mater. Des. 49, 716 (2013).

22. C. Cheng, B. Yu, Z. Chen, and J. Liu, J. Mater. Sci. Technol. (2018).

23. J. Li, J. Shen, S. Hu, H. Zhang, and X. Bu, Opt. Laser Technol. 109, 123 (2019).

24. K. Zhang, Z. Lei, Y. Chen, M. Liu, and Y. Liu, Opt. Laser Technol. 73, 139 (2015).

25. C. Y. Chu, C. T. Hsieh, and L. W. Tsay, MATERIALS&DESIGN (2014).

26. L. Tan, Z. Yao, W. Zhou, H. Guo, and Y. Zhao, 14, 302 (2010).

27. S. Q. Wang, W. Y. Li, K. Jing, X. Y. Zhang, W. Y. Li, K. Jing, X. Y. Zhang, and D. L. Chen, Mater. Sci. Eng. A (2017).

28. H. Zhang, P. He, J. Feng, and H. Wu, Mater. Sci. Eng. A 425, 255 (2006).

29. H. Zhang, S. Hu, J. Shen, D. Li, and X. Bu, Opt. Laser Technol. 74, 158 (2015).

30. W. A. B. Iii and J. Hurley, 175 (n.d.).

31. V. E. Yeganeh and P. Li, Mater. Des. 124, 78 (2017).

32. Q. Chu, M. Zhang, J. Li, C. Yan, and Z. Qin, Influence of Vanadium Filler on the Properties of Titanium and Steel TIG Welded Joints (Elsevier B.V., 2016).

33. I. Tomashchuk, P. Sallamand, H. Andrzejewski, and D. Grevey, Intermetallics 19, 1466 (2011).

34. a De and T. DebRoy, Sci. Technol. Weld. Join. 16, 204 (2011).

35. M. J. Tan, G. W. Chen, and S. Thiruvarudchelvan, J. Mater. Process. Technol. 192, 434 (2007).

36. T. Ahmed and H. J. Rack, Mater. Sci. Eng. A 243, 206 (1998).

37. L. Zeng and T. R. Bieler, Mater. Sci. Eng. A 392, 403 (2005).

38. R. Filip, K. Kubiak, W. Ziaja, and J. Sieniawski, J. Mater. Process. Technol. 133, 84 (2003).

39. G. F. Vander Voort, S. R. Lampman, B. R. Sanders, G. J. Anton, C. Polakowski, J. Kinson, K. Muldoon, S. D. Henry, and W. W. Scott Jr, Metallogr. Microstruct. 9, 44073 (2004).

40. T. Kelly, W. Cremisio, and W. Simon, Weld. J. 68, 14 (1989).

41. K. Saida, A. Taniguchi, H. Okauchi, H. Ogiwara, and K. Nishimoto, Sci. Technol. Weld. Join. 16, 553 (2011).

42. K. Saida, K. Ohta, and K. Nishimoto, Sci. Technol. Weld. Join. 12, 593 (2007).

43. Astm-E2546-07, Astm E2546-07 1, 1 (2007).

44. J. Jang, 10, 391 (2009).

45. L. N. Zhu, B. S. Xu, H. D. Wang, and C. B. Wang, Crit. Rev. Solid State Mater. Sci. 40, 77 (2015).

46. N. S. Rossini, M. Dassisti, K. Y. Benyounis, and A. G. Olabi, Mater. Des. 35, 572 (2012).

47. P. Xie, H. Y. Zhao, B. Wu, and S. L. Gong, Acta Metall. Sin. (English Lett.) 28, 922 (2015).

48. J. X. Zhang, Y. Xue, and S. L. Gong, Sci. Technol. Weld. Join. 10, 643 (2005).

49. B. Appolaire, A. Settefrati, and E. Aeby-Gautier, Mater. Today Proc. 2, S589 (2015).

50. R. J. Moat, H. J. Stone, A. A. Shirzadi, J. A. Francis, S. Kundu, A. F. Mark, H. K. D. H. Bhadeshia, L. Karlsson, and P. J. Withers, 16, 279 (2011).

**Tables and Figures**

**Table 1** Parameters for dissimilar pulsed TIG welding of Ti-5Al-2.5Sn/cPTi

| S. No | Current | | Pulse width | | Voltage | Welding speed | Filler alloys |
|---|---|---|---|---|---|---|---|
| | Primary | Background | High | Low | | | |
| 1 | 32 A | 16 A | 8 ms | 4 ms | 10 V | 32.5 mm/min | - |
| 2 | 32 A | 16 A | 8 ms | 4 ms | 10 V | 32.5 mm/min | cpTi |
| 3 | 32 A | 16 A | 8 ms | 4 ms | 10 V | 32.5 mm/min | Ti-5Al-2.5Sn |

**Table 2** Stress-strain characteristics of the smooth tensile testing of Ti-5Al-2.5Sn/cpTi weld joints.

| Sample | Maximum Load (N) | Energy at Break (J) | Extension at Break (mm) |
|---|---|---|---|
| No filler wire | 3658 | 4 | 2 |
| Ti-5Al-2.5Sn filler wire | 3668 | 15 | 5 |
| cpTi filler wire | 3757 | 21 | 7 |

**Table 3** Stress-strain characteristics of notch tensile specimen of Ti-5Al-2.5Sn/cpTi weld joint.

| Sample | Maximum Load (N) | Energy at Break (J) | Extension at Break (mm) |
|---|---|---|---|
| No filler wire | 5248 | 10 | 3 |
| Ti-5Al-2.5Sn filler wire | 5600 | 16 | 3 |
| CP-titanium filler wire | 5896 | 29 | 6 |

**Table 4** Summary of the nano-mechanical properties of the Ti-5Al-2.5Sn/cPTi weld joint for different conditions of filler.

| S.No | Type of filler | Nano-hardness (GPa) | | | | Elastic Modulus (GPa) | | | |
|---|---|---|---|---|---|---|---|---|---|
| | | BM cpTi | HAZ cpTi side | FZ | HAZ of Ti-5Al-2.5Sn side | BM Ti-5Al-2.5Sn | HAZ of cpTi side | FZ | HAZ of Ti-5Al-2.5Sn side |
| 1. | No filler | | 2±0.1 | 3±0.1 | 5±0 | | 120±9 | 128±3 | 145±4 |
| 2. | cpTi | 2.0±0.3 | 2±0.4 | 3.6±0.8 | 4±0 | 4.5±0.4 | 123±7 | 134±4 | 140±9 |
| 3. | Ti-5Al-2.5Sn | | 2±0.5 | 4±0.3 | 4±0 | | 113±3 | 139±1 | 136±5 |

**Table 5**. Longitudinal and transverse residual stresses in the Ti-5Al-2.5Sn/cPTi weld joint for different conditions of filler.

| S. No | Type of filler | Depth (mm) | Longitudinal residual stresses (MPa) | | Transverse residual stresses (MPa) | |
|---|---|---|---|---|---|---|
| | | | cpTi side | Ti-5Al-2.5Sn side | cpTi side | Ti-5Al-2.5Sn side |
| 1. | No filler | 0.1 | 63 | 130 | 89 | 85 |
| | | 0.7 | 30 | -43 | 46 | 20 |
| 2. | cpTi | 0.1 | -2 | -53 | 107 | 61 |
| | | 0.7 | -35 | -23 | 74 | 150 |
| 3. | Ti-5Al-2.5Sn | 0.1 | 99 | -177 | 69 | -148 |
| | | 0.7 | 56 | -169 | 18 | -111 |
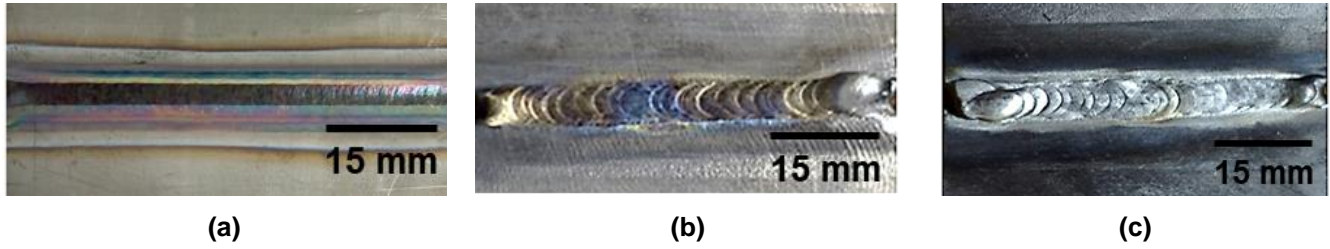
**Fig. 1** Physical appearance of the weldments with (a) no filler, (b) Ti-5Al-2.5Sn filler wire and
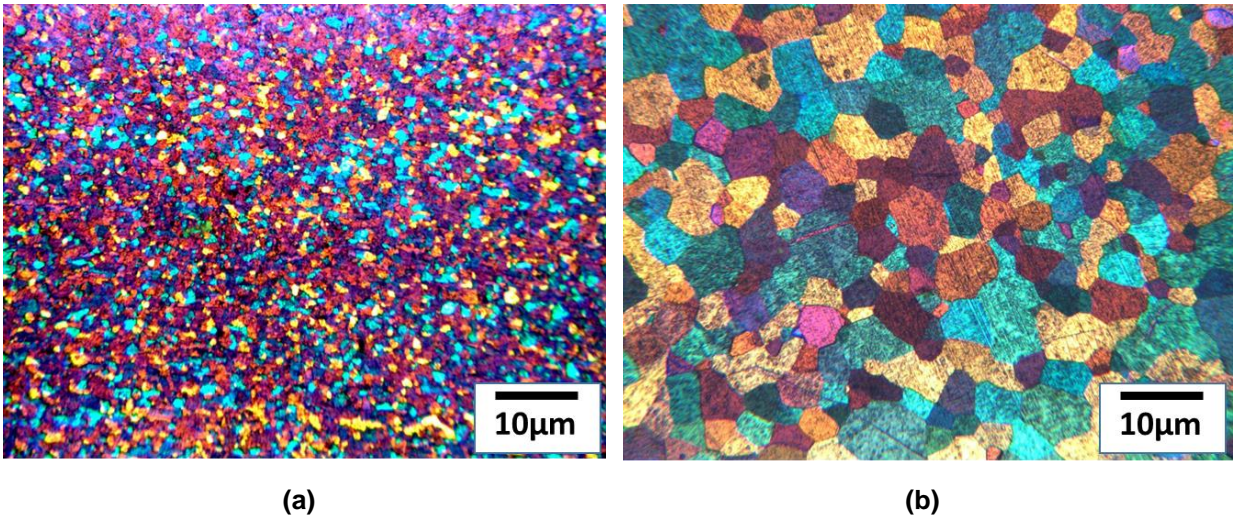
(c) cpTi filler wire.



**Fig. 2** Microstructure of the two base metals: (a) Ti-5Al-2.5Sn (b) cpTi.
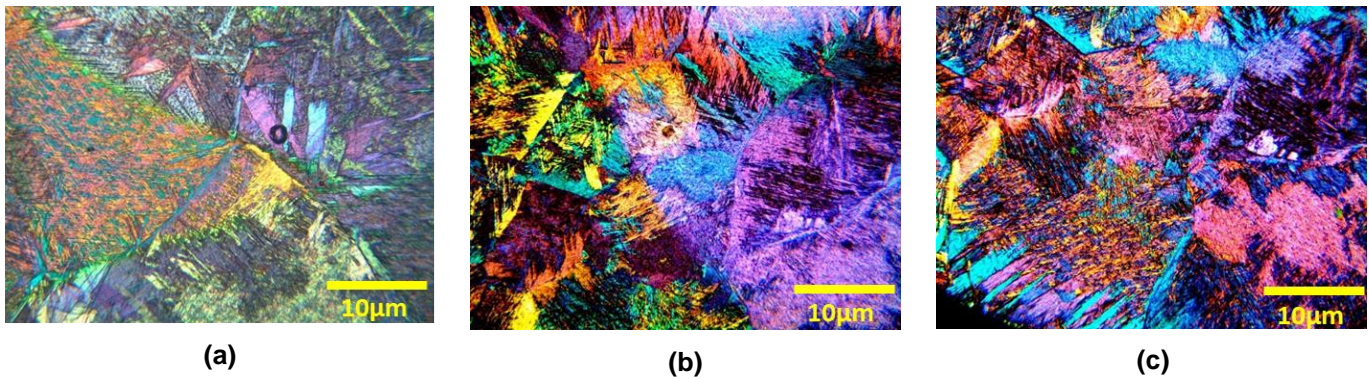


**Fig. 3** Microstructure of FZ in the Ti-5Al-2.5Sn/cpTi dissimilar alloy weldments with (a) No

filler, (b) Ti-5Al-2.5Sn filler wire and (c) Cp-Ti filler wire.

25
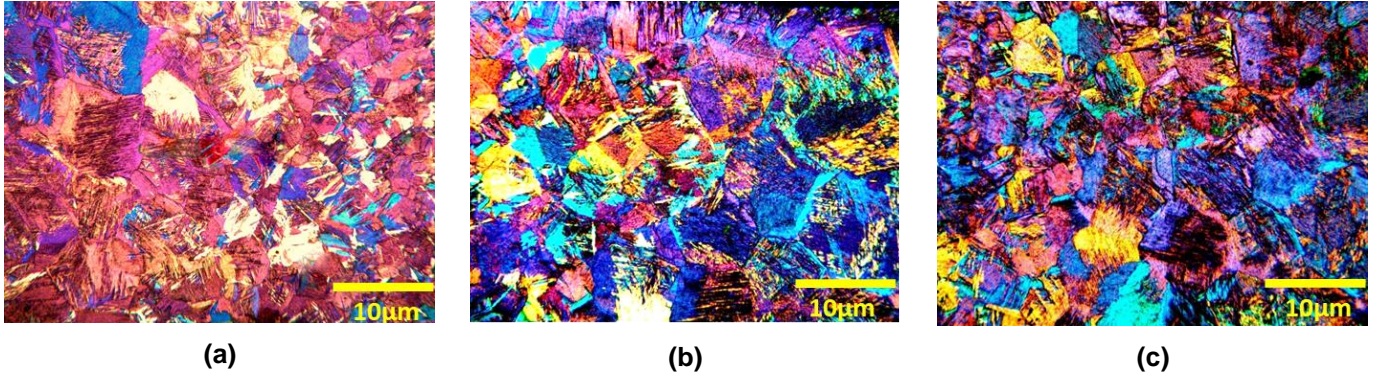
**Fig. 4** Microstructure of HAZ towards Ti-5Al-2.5Sn side in the Ti-5Al-2.5Sn/cpTi dissimilar

alloy weldments with (a) No filler, (b) Ti-5Al-2.5Sn filler wire and (c) Cp-Ti filler wire.
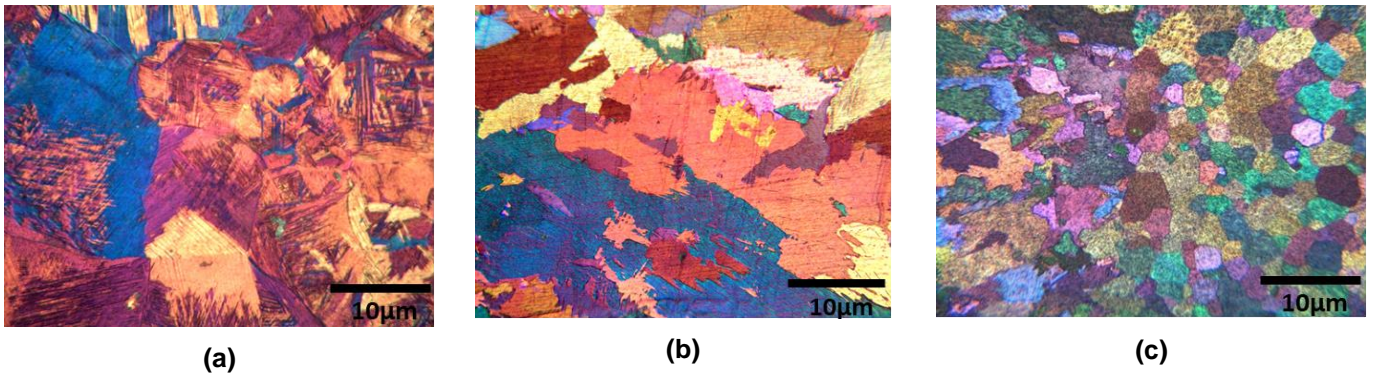


**Fig. 5** Microstructure of HAZ towards cpTi side in the Ti-5Al-2.5Sn/cpTi dissimilar alloy

weldments with (a) No filler, (b) Ti-5Al-2.5Sn filler wire and (c) Cp-Ti filler wire.
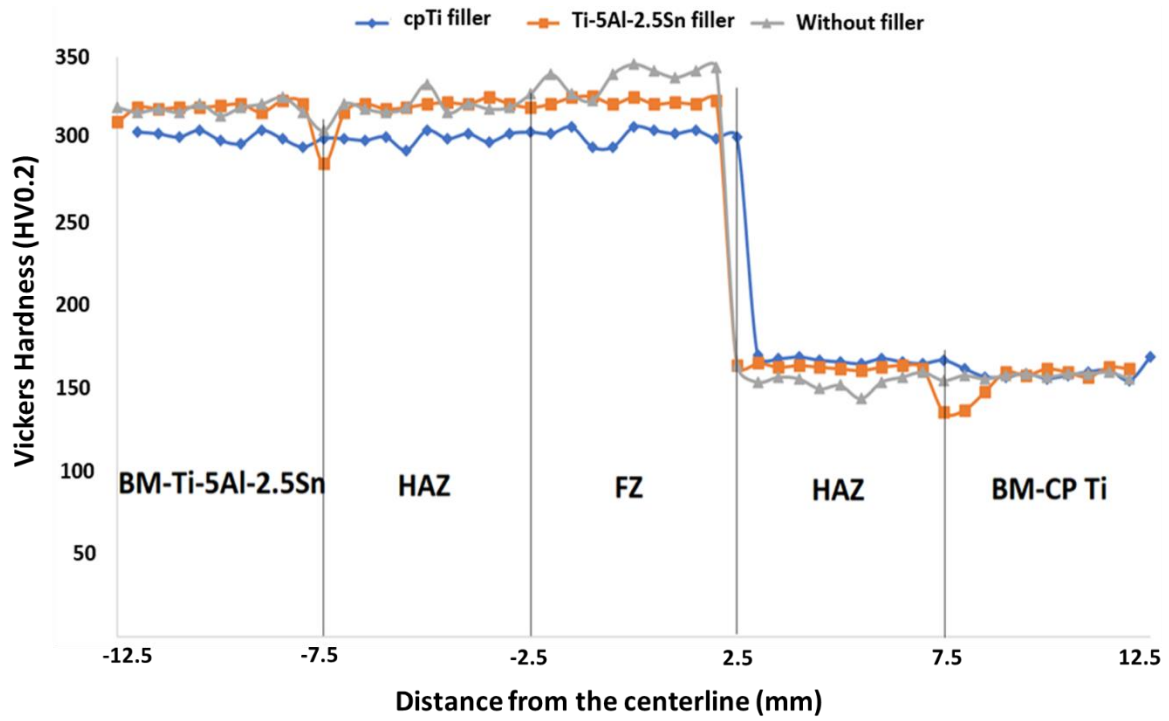
**Fig. 6** Micro hardness profiles across the Ti-5Al-2.5Sn/cPTi weld joints for different conditions of fillers.
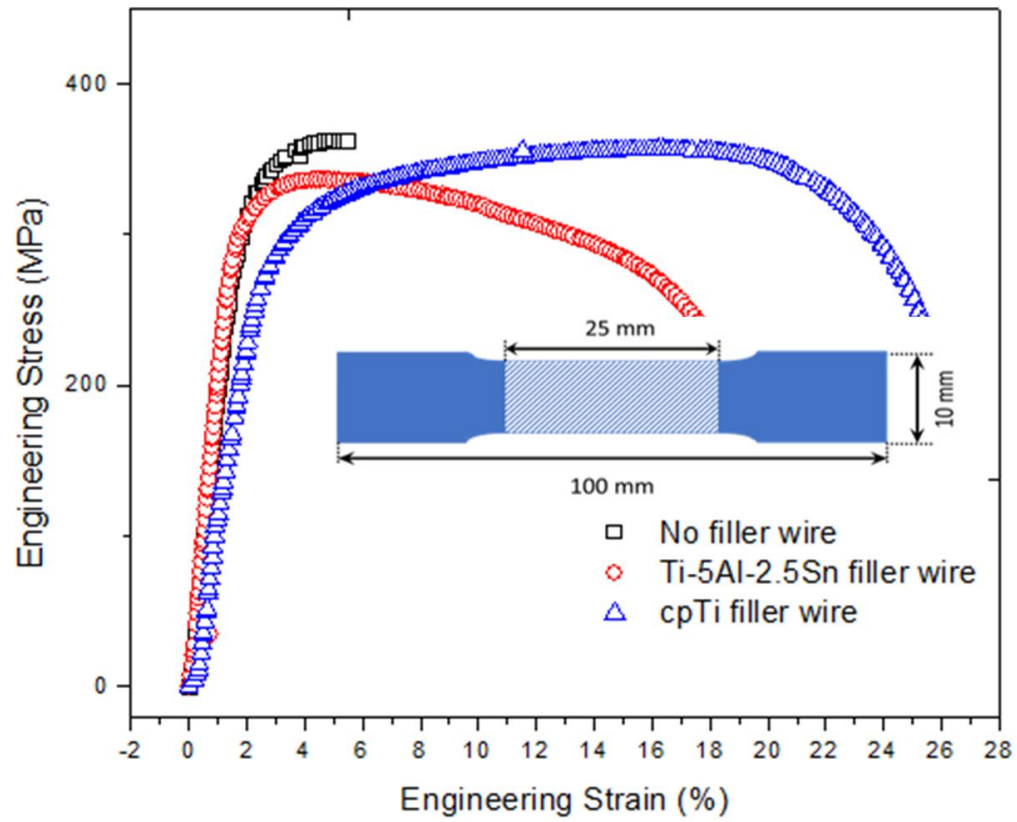
**Fig. 7** Stress-strain curve of the smooth tensile specimen of Ti-5Al-2.5Sn/cpTi weld joint for

different conditions of filler material.
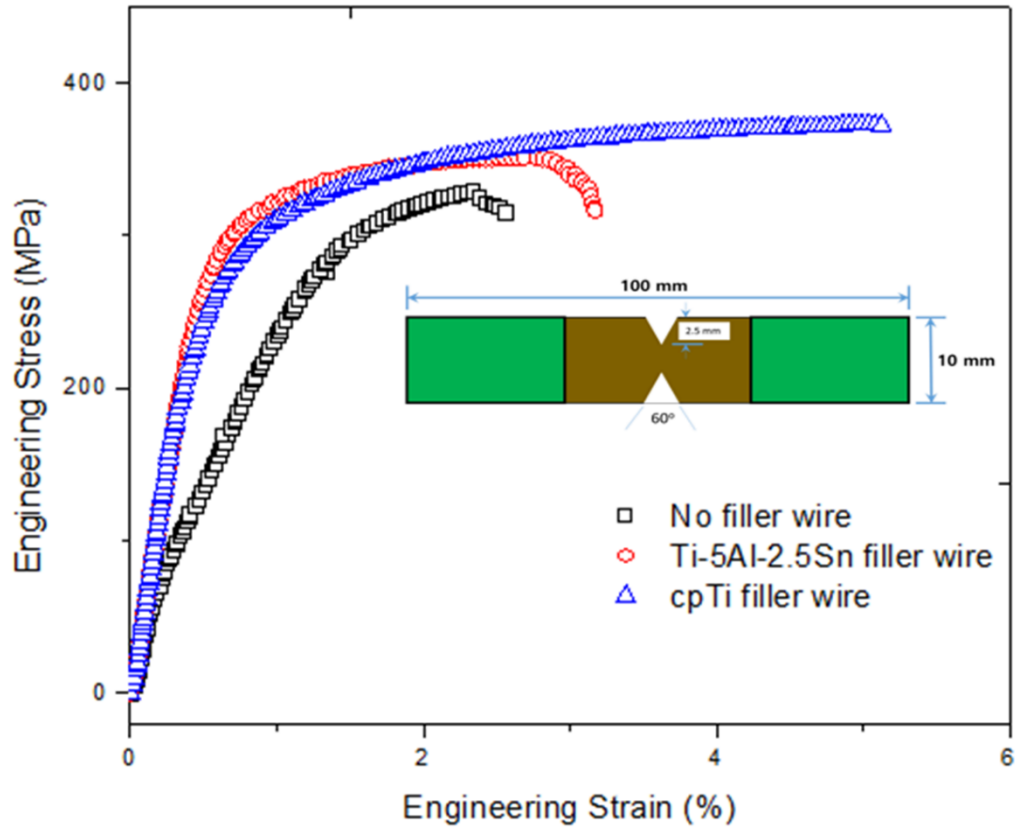
**Fig. 8** Stress-strain curve of the notch tensile specimen of Ti-5Al-2.5Sn/cpTi weld joint for

different conditions of filler material.



| (a) | (b) | (c) |
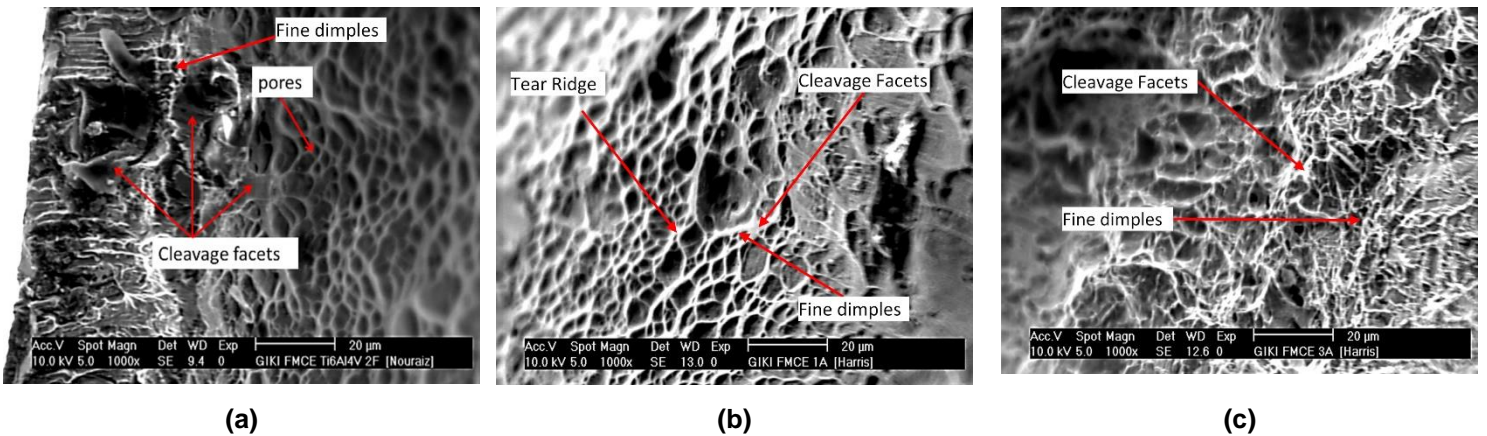
**Fig. 9** SEM factographs of the fractured surfaces of double notch tensile specimens of Ti-5Al-

2.5Sn/cpTi dissimilar weldments with (a) no filler, (b) Ti-5Al-2.5Sn filler and (c) cpTi filler.
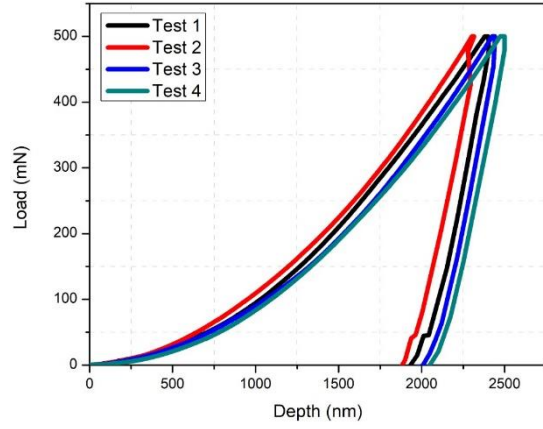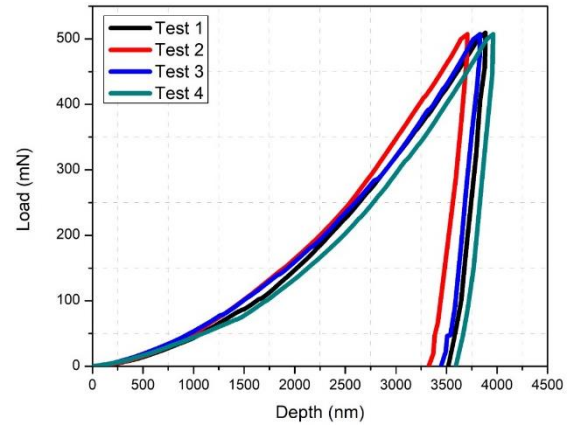
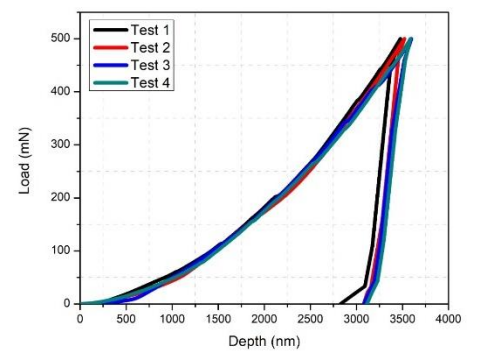**Fig. 10** Nano indentation Load-depth curves of the base materials: (a) Ti-5Al-2.5Sn (b) cp-Ti.
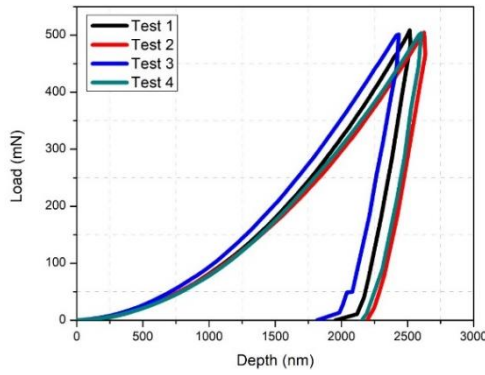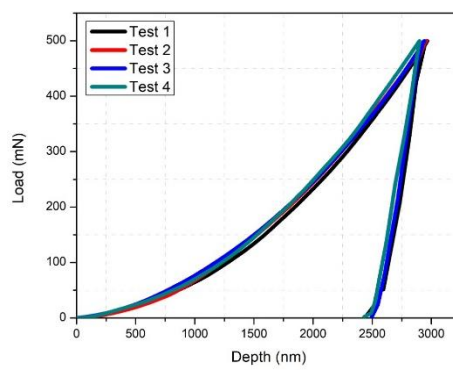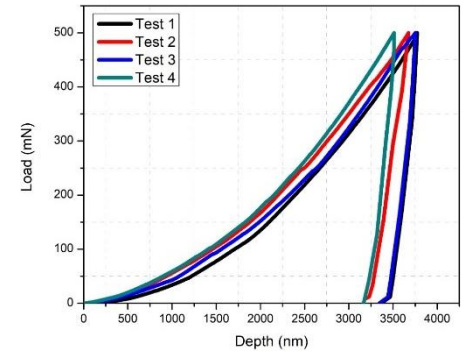


**Fig. 11** Nano indentation Load-depth curve of the weldments without filler material (a) HAZ of
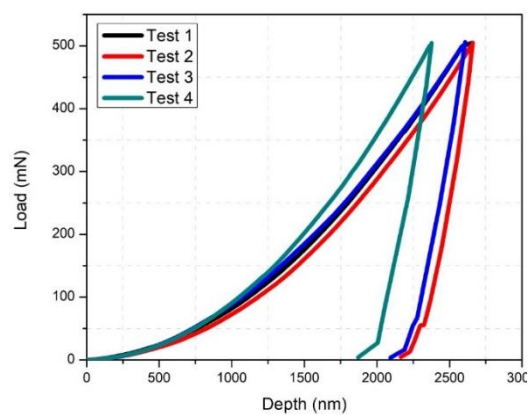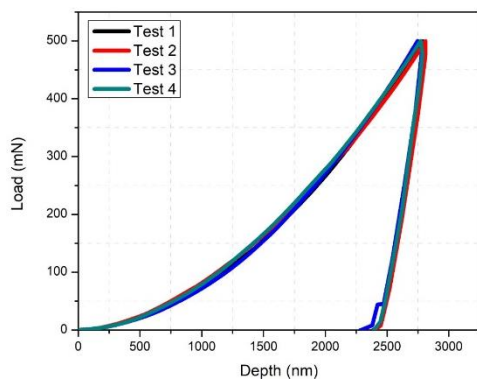
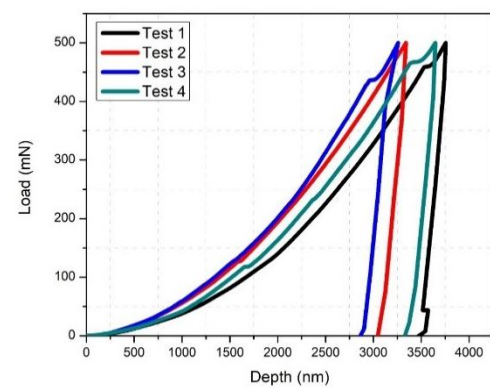Ti-5Al-2.5Sn side (b) FZ (c) HAZ of cpTi side
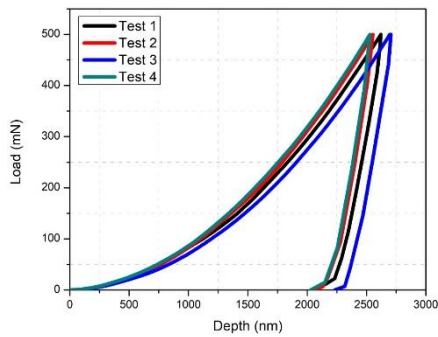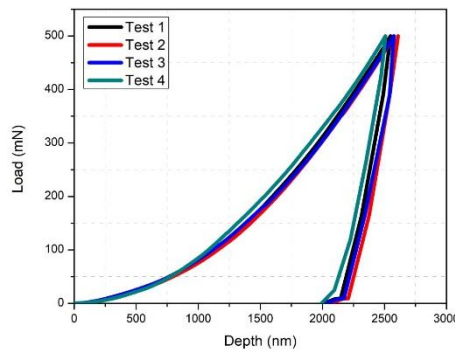


**Fig. 12** Nano indentation Load-depth curve of the weldments obtained using Ti-5Al-2.5Sn wire

filler (a) HAZ of Ti-5Al-2.5Sn side (b) FZ (c) HAZ of cpTi side

**Fig. 13** Nano indentation Load-depth curve of the weldments obtained using cpTi wire filler (a)

HAZ of Ti-5Al-2.5Sn side (b) FZ (c) HAZ of cpTi side